3D printing of jammed self-supporting microgels with alternative mechanism for shape fidelity, crosslinking and conductivity

Additive Manufacturing 58 (2022) 102997

Contents lists available at ScienceDirect

Additive Manufacturing

journal homepage: www.elsevier.com/locate/addma

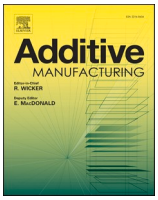

3D printing of jammed self-supporting microgels with alternative mechanism for shape fidelity, crosslinking and conductivity

Mehdi Sheikhi [a], Fatemeh Rafiemanzelat [a,*], Saman Ghodsi [b], Lorenzo Moroni [c], Mohsen Setayeshmehr [d]

[a] Polymer Chemistry Research Laboratory, Department of Chemistry, University of Isfahan, Isfahan 81746-73441, Islamic Republic of Iran
[b] Department of Plant and Animal Biology, Faculty of Biological Science and Technology, University of Isfahan, Isfahan 81746-73441, Islamic Republic of Iran
[c] MERLN Institute for Technology Inspired Regenerative Medicine, Complex Tissue Regeneration Department, Maastricht University, Universiteitssingel 40, 6229ER Maastricht, the Netherlands
[d] Biomaterials and Tissue Engineering Department, School of Advanced Technologies in Medicine, Isfahan University of Medical Sciences, Isfahan 81746-73461, Iran

ARTICLE INFO

Keywords:
Jammed microgels
3D printing
Deep eutectic solvent
Crosslinking
Conductivity

ABSTRACT

Additive manufacturing technology is a growing field, which demands advanced chemistry and fabrication process if smart-materials are desired. Herein, the concept of jammed microgels designed with a new crosslinking method is introduced to be used in 3D-printing applications. Jammed microgels decorated with superficial hydrophobic segments and pure thermo-sensitive gelatin are applied as inks and exhibit shear-induced transition and fast recoverability, which are important for 3D-printing. The interaction of microgels within the as-extruded filaments and with the adjacent deposited layers guarantees shape-fidelity. After printing, a deep eutectic solvent (DES) formed from Arginine and Glycerol ($[DES]_{Arg/Gly}$) is applied over the construct to trigger a chemical crosslinking reaction between epoxy and amine groups. The introduced $[DES]_{Arg/Gly}$ can play simultaneously two roles: (1) activator of covalent bond formation and (2) conducting agent. Generally, a variety of features including printability, rheological properties and shape-retention are dependent on the fraction of hydrophobic segments and the applied $[DES]_{Arg/Gly}$ concentration. Further, the main network percolation reaction follows a different strategy to achieve a sustainable printable system with biological, mechanical and physiological sustainability of the construct. These results open new possibilities to fabricate a wide range of adaptive platforms of smart materials with ease.

1. Introduction

Three-dimensional (3D) printing has been adopted by different research groups and industries due to its potential to fabricate complex constructs with desired dimensions, geometry, and architecture [1]. Among different fabrication strategies, extrusion-based 3D printing has been the most attractive due to their feasibility and affordability [2,3]. The configuration of these systems consists of several cartridges through which the ink is ejected as a filament, typically by applying pressure. Selecting a material as the biomaterial ink is key and restrictive factor to achieve an ideal construct, because a demanding set of requirements are connected directly to the type and properties of precursors and chemical reactions [4–6]. In addition, from the point of view of biological applications, the ink must meet the criteria of cellular responsiveness to achieve a versatile platform [7]. A great effort is currently being made to optimize the chemistry of materials to provide: (i) processability and printability, (ii) high fidelity and (iii) network formation through a reaction with adequate biocompatibility [8–10].

Recent studies have assessed the relationship between printability and rheology of long polymer chains either by mathematical models or by analyzing the physical appearance of ejected filaments [11,12]. Although the found property–function relationships enable a more rational approach optimizing the material's printability and resolution, when cell-laden hydrogels are used the shear stress experienced by the cells during extrusion could affect cell activity, resulting in poor cell viability. To tackle this problem, manipulating the ink composition or modification of the polymer backbone are common methodologies to provide a fast break-recovery characteristic [13]. The development of the inks based on jammed particles is a novel and motivating approach to control the printability of the components and modulate desired

* Corresponding author.
E-mail address: frafiemanzelat@chem.ui.ac.ir (F. Rafiemanzelat).

https://doi.org/10.1016/j.addma.2022.102997
Received 17 January 2022; Received in revised form 15 June 2022; Accepted 26 June 2022
Available online 29 June 2022

physico-chemical characteristics of the resulting constructs more efficiently [14–16]. Moreover, jammed structures not only provide micron-size pores for cellular infiltration to enhance cell viability, attachment and migration, but also can improve extrudability due to the physical nature of aggregation and the shear thinning behavior of aggregates. Microgels in a jammed state are absorbed by adjacent particles through secondary interactions and exhibit a solid-like behavior until the applied stress overloads the yield stress [17]. Such interactions can provide shear thinning and shear recovery properties, a major advantage compared to the bulk liquid inks. These interactions should be tailored to meet the flow and recovery demands. Otherwise, either the ink cannot be printed or the needed flow properties and construct fidelity are compromised. Till now, several (jammed) ink precursors have been introduced that solidify using either photo illumination (covalent crosslinking) or formation of secondary interactions [18–20]. The first suffers from the occurrence of cell death upon exposure to high-energy rays. To form secondary and transient interactions, different strategies like light polymerization, coordination chemistry [21,22], thiol- ene crosslinking [23,24], supramolecular interactions [25], and dynamic covalent chemistry [26] are adopted to accelerate network formation. Depending on the nature of the interactions, these strategies present various limitations such as mechanical weakness, needing for long time recovery after break, degradation in the culture media, diffusibility, expandability, and problems associated with creep phenomenon, all highly timescale dependent [26,27].

In this study, we introduced the new concept of jammed microgels aggregated via a novel crosslinking system. Aimed at this, gelatin microgels (Mgels) comprising superficial hydrophobic interactions were recruited, which provide self-supporting filaments due to the presence of satisfactory interactions between the extruded microgels [28]. A mixture (G-gel) of Mgels with pure thermo-sensitive gelatin molecules can present stable filaments with self-supporting characteristics and high fidelity after deposition. To chemical crosslink the 3D printed constructs, the application of deep eutectic solvents (DESs) is introduced to trigger covalent bond formation. DESs are a class of polar materials obtained by the interaction of two or more compounds with hydrogen bonding donor (HBD) and hydrogen bonding acceptor (HBA) characteristics and are considered as promising materials because of their superior properties and functionalities and can be applied as high-efficient catalysts, solvents, precursor or conducting agents [29–31]. According to our recent report, DESs based on aminoacids and 1,2-diols are highly efficient to make epoxy functional groups susceptible for nucleophilic reactions [32]. The introduced DES in the present study is based on L-arginine and glycerol, namely ($[DES]_{Arg/Gly}$), which performs as a catalyst to trigger fast chemical crosslinking at ambient conditions, and as a conductive agent to fabricate electrically conductive 3D printed soft materials as well. Conductive hydrogels have attracted special attention due to their broad range of applications including electrical stimulation of cells [33], in nerve [34], muscle [35] and cardiovascular [36] tissue engineering. Conducting polymers such as polypyrrole, polyaniline and polythiophene are widely used biomaterials in tissue engineering applications due to their electrical properties. However, they suffer from weak mechanical properties and poor biocompatibility and processability [37,38]. Incorporation of metal nanoparticles and carbon-based materials has emerged as an alternative approach, but the conductivity of the material compromised by random distribution of nanomaterials or coagulation of particles [37,39]. Therefore, the unique properties of DESs make them interesting substances for the fabrication of smart materials for tissue engineering applications. Hence, the findings of this work open an interesting and promising new method to fabricate 3D printed constructs with ease and in an adjustable manner.

2. Experimental section

2.1. Materials

Gelatin powder (bovine gelatin), acrylic acid and ammonium peroxodisulfate were provided from Merck (Germany). L-arginine (≥98%) (Arg), glycidyl methacrylate (GMA), emulsifier span 60 and 4′,6-diamidino-2- phenylindole (DAPI) were obtained from Sigma-Aldrich used without purification. Glycerol (Gly) was also supplied from Merck and dried under vacuum at the temperature of 70 ℃ before use in the DES synthesis reaction.

2.2. Preparation of microgels Mgel $_{I}$, Mgel $_{II}$, Mgel $_{III}$ and Ink

The microgels are prepared according to our previous work [28]. In brief, for preparation of Mgel $_{II}$ and Mgel $_{III}$, a reverse emulsion polymerization protocol was performed by dropping an aqueous solution containing vinyl-functionalized gelatin, acrylic acid and an initiator (ammonium persulfate) into an oil phase containing water-insoluble glycidyl methacrylate monomer. Mgel $_{I}$ was synthesized by the same procedure except that the continuous phase was free of GMA monomer; thus, Mgel $_{I}$ does not contain hydrophobic PGMA chains, but Mgel $_{II}$ and Mgel $_{III}$ carry these segments with the difference that the segments are longer in the case of Mgel $_{III}$. The length of the PGMA segment was controlled via concentration of glycidyl methacrylate monomer used in the oil phase of the emulsion reaction. Determination of the epoxide value confirmed the presence of longer segments of Mgel $_{III}$ compared to Mgel $_{II}$ as detailed in literature [28]. Finally, the microgels were centrifuged and then washed 2 times with distilled water, 5 times with ethanol: distilled water (40:60 v/v) solution, and again 2 times with distilled water. The sequence and volume of ethanol should be precisely controlled as the coagulation of microgels will occur, especially if the volume of ethanol exceeds this ratio.

For preparation of material inks, the microgels were kept at the 50 ℃ to decrease the water content up to 1400% w/w of the particles. Then, the ink was prepared following dissolving pure gelatin (20% w/w) at 40 ℃ with the obtained microgels. The samples are coded as G-gel $_{I}$, G-gel $_{II}$ and G-gel $_{III}$, prepared based on microgels Mgel I to III, respectively.

2.3. Synthesis of DES $[DES]_{Arg/Gly}$

The deep eutectic solvent was formed by mixing Arg and Gly at different molar ratios 1:0.5, 1:1, 1:2, 1:3, 1:4, and 1:5, and heating the mixtures at 120 °C to obtain a homogeneous yellowish-brown liquid. Next, the temperature was decreased to 50 °C and the mixture was continued to be mixed for 20 min. Fresh mixtures were characterized to determine proper molar ratios to achieve an eutectic mixture. The as-prepared DES was applied in the crosslinking reaction, since the activity of DES diminishes after few hours (15–16 h) of preparation.

2.4. Printing system and printing condition

Additive manufacturing of the microgels was carried out by a homemade extrusion printer. The ink was transferred into the cartridge assembled with the heated printhead at the temperature of 48 ℃. The prepared ink was extruded from a 18 gauge nozzle through a pressure driven piston. Printing was performed on a glass substrate using a tip travel speed of 2 mm/s. After printing, the construct was exposed to fresh pure $[DES]_{Arg/Gly}$ or $[DES]_{Arg/Gly}$ aqueous solution (50:50 v/v) for chemical crosslinking, and a stable structure was obtained after 2–3 min

2.5. Rheological characterization

Rheological properties were characterized using a rheometer with 8 mm diameter parallel plate steel geometry. The gap was 1 mm and the measurements were performed at 25 ℃. To explore shear-thinning

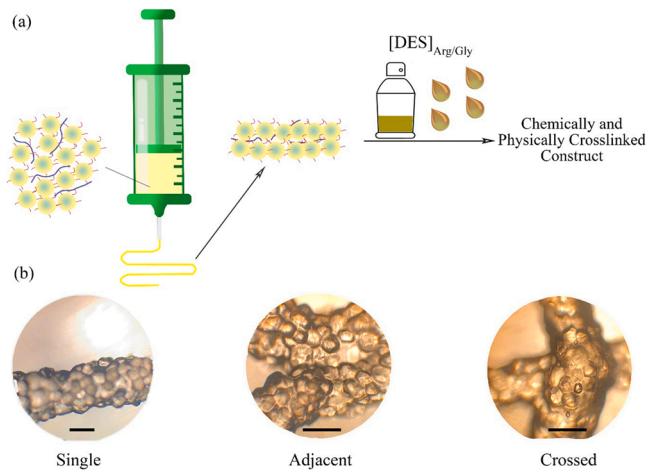

Fig. 1. (a) Scheme of 3D printing process based on jammed microgels, its extrusion and chemical crosslinking. Particle jamming occurs when the water content in the system decreases below a critical point in which the PGMA segments over the particles provide contact forces between the neighboring microgels. After extrusion, gelatin molecules (blue lines) convert to gel state and the strength of the material is increased. In the next step, $[DES]_{Arg/Gly}$ can be applied either in pure state or spraying aqueous solution to trigger chemical crosslinking reaction. (b) The images of the extruded ink under an optical microscope in three common positions used in additive manufacturing process. Scale bar is 200 μm.

properties, the viscosity was measured at shear rates 0.1–100 s^{-1} and strain sweep in the range 1–100% was performed at an angular frequency of 10 rad/s. Self-healing measurements were performed at four cycles 10 rad/s, including 200 and 400 s at 0.1% strain with 5 s at rest (0% strain) between each step. To explore the stability of printed constructs and sol-gel transition behavior, a temperature sweep was performed at a temperature of 25–50 ℃, a strain of 1% and a frequency of 1 Hz. Creep experiments were carried out by applying a constant stress ($\tau = 50$ Pa) for 1200 s at the temperature of 25 ℃ and the corresponding strain was measured. Kinetic investigation was performed at a strain amplitude of 10% and a frequency of 1 Hz. In order to investigate the viscoelastic properties of the chemically crosslinked samples, G' and G'' were recorded as a function of frequency over the range 0.1–100 Hz at 0.5% strain.

2.6. Measurements of mechanical properties

Compression tests were performed on a Santam 5567 electronic universal testing machine. For this, cylindrical specimens with 10 mm height and 18 mm diameter were subjected to compression test and the corresponding force was measured. The experiments (n = 3) were carried out at room temperature using a machine equipped with a 500 N load cell at a rate of 1.0 mm/min. Specimens were preloaded to ensure proper seating of the plate on the specimen surface. The uniaxial elongation properties were measured using Zwick 1446 (Germany). The procedure was as follows: in a rectangular-shaped mold with a dimension of 80 mm × 30 mm × 3 mm, the filaments were deposited once along the length of the mold (for samples where the orientation of the filaments is parallel to the direction of tensile stress) and along the width of the rectangle (for samples where the orientation of the filaments is perpendicular to the direction of tensile stress). Hydrogels were cut in a dumbbell shape with a 75 mm length, 25 mm gauge length, 3 mm width and tests were conducted at cross-head speed of 10 mm/min.

2.7. Structure characterization

2.7.1. Fourier transform infrared spectroscopy (FT-IR) and nuclear magnetic resonance spectroscopy (^{1}H NMR)

Infrared spectra were obtained on FT-IR 0066 Spectrophotometer, Jasco (Japan), in the range of 4000–400 cm^{-1}. The samples were supported on transparent KBr films to obtain the spectra. For kinetic measurements, the scan was recorded immediately after mixing the reaction precursors. For ^{1}H NMR measurements, the synthesized DES and mixture of DES components were dissolved separately in D_2O and the spectra were obtained using a Bruker (Germany) Advance 400 MHz spectrometer.

2.7.2. Scanning electron microscopy (SEM)

In order to observe morphology and porosity of the 3D printed constructs, the samples were immersed in water to reach equilibrium and then lyophilized and cut in liquid nitrogen. Next, the cross section of specimens was sputter-coated with gold (30 mA, 20 s) using an auto sputter-coater (Cressington 108) and then inspected by means of a Hitachi S4700 SEM at an accelerating voltage of 20 kV.

2.8. Swelling ratio

For the swelling evaluation, the samples were immersed in distilled water at room temperature for 24 h. Then, the sample were weighed in wet condition (W_w) and let it to dry until a constant weight was reached (W_d). A swelling ratio was calculated as Eq. (1):

$$100 \times (W_w - W_d)/W_d \quad (1)$$

The measurements were repeated three times to calculate the average and standard deviation.

2.9. Biodegradability

The degradation profile of 3D printed constructs crosslinked with two concentrations of $[DES]_{Arg/Gly}$ was evaluated by immersing the specimens in phosphate-buffered saline at 37 °C. The percentage of weight loss was measured at different time points according to the procedure reported in literature [40].

2.10. Cell viability

The murine fibroblast cell line L929 was obtained from the Pasteur institute cell bank (Tehran, Iran); COCA, a murine epidermal cell line, was developed by serially passaging of the keratinocytes from the back skin of adult C57BL/DBA mice. The Institutional Ethics Committee of University of Isfahan approved the informed consent for animals and the study. The cells were cultured in supplemented Dulbecco's minimal Eagle medium (DMEM_F12), 10% fetal bovine serum (FBS; Gibco), 1% penicillin-streptomycin (Bioidea, Iran) at 37 °C in a humidified atmosphere containing 95% air and 5% CO_2. The relative viability of encapsulated Fibroblast and Keratinocyte cells (1×10^4 cells/sample) were evaluated by the 3-(4, 5-Dimethyl-2-thiazolyl)− 2, 5-diphenyl-2 H-tetrazolium bromide (MTT, Sigma) assay at day 7 of the culture. For this, the cells were resuspended in culture media (cell density, 2×10^5 cells/mL) and mixed with G-gel $_{III}$ (0.05 mL cell suspension/1 g G-gel $_{III}$). The resulted bioink was transferred into a syringe and extruded via a 16 gauge nozzle by applying pressure. Following extrusion, 1% w/w $[DES]_{Arg/Gly}$ was poured on the sample. Finally, the MTT assay was performed according to the previous study and the optical density (OD) was measured at 490 nm using a plate reader (Hyperion MPR4) [28].

2.11. Electrical stimulation experiment

A simple homemade electric field setup was built on the Petri dish in order to evaluate the performance of DES as a green conducting agent to

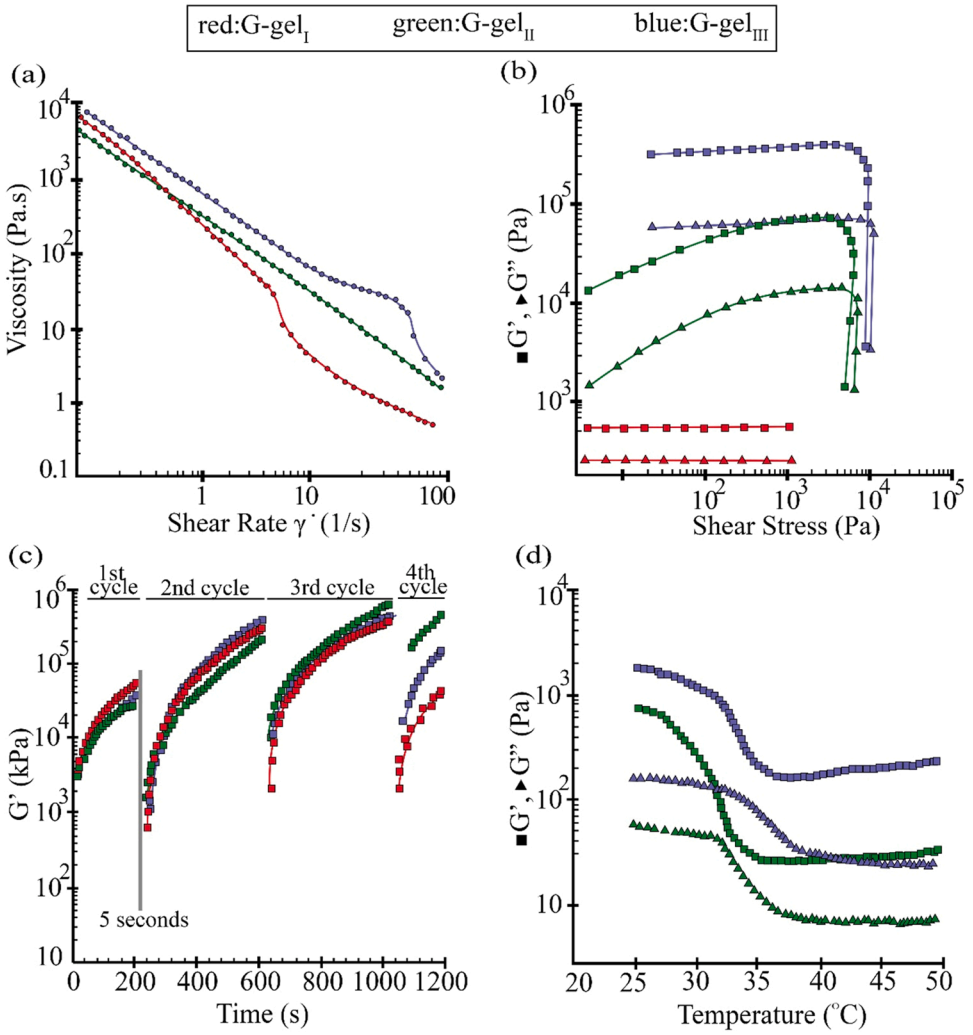

Fig. 2. Rheological characterization of gelatin jammed microgels. (a) Apparent viscosity decreases for three ink systems under steady shear. (b) Measurement of yield stress for the inks at 0.1–100% strain range. (c) Evaluation of the self-recovery property of inks in terms of the performance of microgels attractions. G-gel $_I$ weakens after experiencing three strain-relaxation processes while G-gel $_{II}$ and G-gel $_{III}$ retain their viscoelastic properties. (d) Variation of G-gel $_{II}$ and G-gel $_{III}$ modulus when the gelatin helical molecules convert to single coil measured at 25–50 ℃, angular frequency of 1 Hz and an oscillatory strain of 1%. Despite the gelatin transition, storage modulus is higher than loss modulus indicating the material still exhibits solid-like behavior.

produce conducting scaffolds for electrical stimulation experiment. For this, fibroblast and keratinocyte cells were separately mixed with as-prepared ink (1×10^5 cells/5 mL ink) and 0.5 mL of bioink was injected into a plate using a syringe from a 16 gauge nozzle. A current of 0.1 A (10 min/day) was applied via dipping the gold electrode into the sample to perform electrical stimulation. The proliferation was explored by DAPI staining [28]. Adobe Photoshop CC 2015 software was used to remove the undesired background in a way that the cell numbers and shapes remained unaltered. For this, a black layer was applied on the as-obtained image, the cells image was separated from the original image and exhibited on the black layer at their original positions and shapes [28].

2.12. Statistical analysis

The SPSS Statistics software version 22 and Microsoft Office Excel 2013 were used for statistical analysis of data. Swelling ratio, force, stress and module were represented as means ± standard deviations. Paired samples t-Test was used to determine possible significant differences between dependent and independent paired samples. A p-value ≤ 0.05 was considered to be statistically significant (*, for $p < 0.05$; **, for $p < 0.01$ and ***, for $p < 0.001$).

3. Results and discussion

3.1. Microgel ink design and work scheme

The stability and resolution of the 3D printed hydrogels as well as biocompatibility of both materials used and manufacturing process are crucial factors that are entirely related to the sustainability of the process and chemistry of construct formation. Crosslinking is one of the most important processing aspect that needs to be considered, because it affects mechanical stability of the printed construct. Although physical crosslinking pathways can provide a more cell-friendly environment, chemical crosslinking is a requisite to obtain shape stability of the construct. For this purpose, different strategies, such as using Schiff-base compounds [41], coupling and cycloaddition reactions [42,43], hydrazide–aldehyde reactions [44], enzymatic crosslinking [45], among others [46–48] are applied. These methods aren't considered as completely sustainable procedures since they have some drawbacks including oxygen inhibition, shrinkage of printed structures, leakage of the unreacted functional groups, and the generation of inhomogeneities in the network of 3D printed constructs [26]. On the other hand, the printability might be affected negatively if the time and place of crosslinking are not controlled. To address this challenge, we attempted to disclose a fundamentally different method based on applying highly efficient $[DES]_{Arg/Gly}$ through which the network formation occurs fast at ambient environmental conditions. This type of DES is homogeneous and water-soluble, which exhibits high efficiency and selectivity for

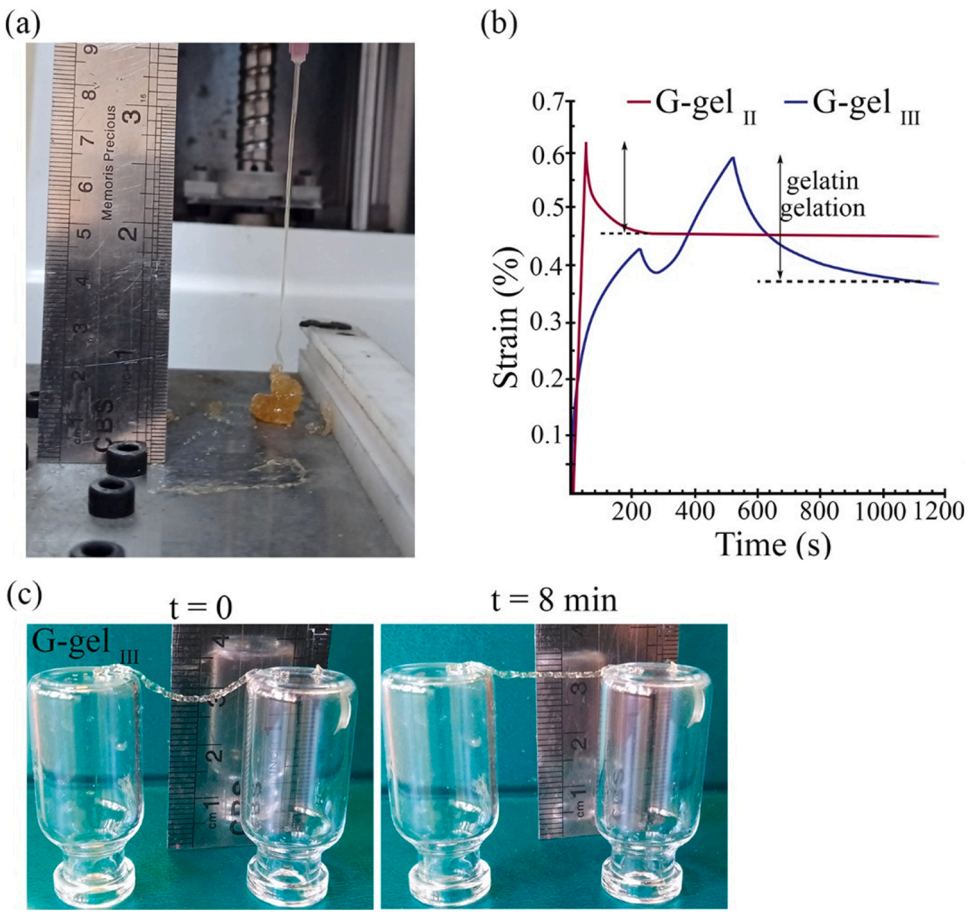

Fig. 3. (a) Stability of the G-gel $_{III}$ filament after extrusion which keeps its own weight without failure. (b) Creep behavior of G-gel $_{II}$ and G-gel $_{III}$ measured at 25 °C under 50 Pa shear stress. G-gel $_{III}$ displays a slower strain evolution. (c) Gelation of gelatin molecules occurs after few min of ejection. Before gelation, the microgels (M-gel $_{III}$) make the extruded filament to retain its shape without mechanical weakness or collapsing.

epoxy-amine reaction under hydrated conditions. The desired reaction is based on combining amine groups of gelatin with epoxy groups of hydrophobic PGMA segments, which is accomplished in few seconds in the presence of $[DES]_{Arg/Gly}$. Prior to investigate the chemical crosslinking, the inks must fulfill the printability requirements to achieve desirable printed structures. For this, we used the combination of hydrophobic-assisted jammed microgels and pure gelatin as a thermoreversible material as ink precursors through which the interaction of microgels provides a self-supporting nature, and consequently the shape-retaining capability is enhanced. The attraction of microgels is dependent on the fraction of hydrophobic segments, and jammed Mgel $_{III}$ presented a stronger attraction at the same water content (Movie S-1, Supplementary Information). The process progresses in a way that the ink converts from a low viscose fluid (inside a cartridge) to a physically crosslinked system after extrusion (on a substrate outside the dispensing tip). During extrusion, the microgels attached to each other via hydrophobic interactions, exhibiting a gel to sol transition as the shear stress overcomes the corresponding yield stress and reattach after removing the stress, as shown in Fig. 1. Subsequently, additional crosslinking within the system occurred by physically crosslinking of the gelatin random coils to enhance the mechanical strength. Although the obtained 3D printed construct is tough and strong enough to be removed from the substrate and transported, it needs chemical crosslinking for further practical applications. Thus, in the final step, $[DES]_{Arg/Gly}$ is applied on the printed construct to trigger the chemical crosslinking and stabilizing the final structure.

This shear-thinning behavior is considered as a prerequisite and depends strongly on the fraction of hydrophobic interactions within the structure, as demonstrated by oscillatory rheology measurement (Fig. 2-a). The viscosity–shear rate relationship of the jammed microgels shows a decreasing trend in viscosity with shear rate due to the separation of jammed particles under the applied stress. Therefore, the particles are susceptible to pass through the extrusion tip with ease due to shear-thinning behavior. It was observed that the viscosity value for G-gel $_{I-III}$ increased from 12 to 78 and 101 Pa.s at a shear rate of 5 s^{-1} as the fraction of hydrophobic segments increased over the microgels. Indeed, with the presence and increasing the fraction of hydrophobic segments, the adhesion between particles was consequently increased. Moreover, a low flow point of G-gel $_{II}$ and G-gel $_{III}$ during the strain sweep from 0.01% to 100% was observed, as shown in Fig. 2-b (in terms of the corresponding stress values). The storage modulus was unchanged at a relatively low stresses, but then dropped abruptly when the shear exceeded a critical value, indicating an unjamming state of the particles. The yield strength was around 4 and 8.2 kPa for G-gel $_{II}$ and G-gel $_{III}$, respectively, and the solid-liked sample presented fluid properties under the critical stress applied. For G-gel $_{I}$, the modulus remained constant to the end without experiencing the yield point, which might be attributed to the irreversible tangled cluster formation.

After being extruded, the viscous fluid ink must undergo rapid transition to a solid-like material to achieve a good printing resolution and shape fidelity. This can be realized if the ink stabilizes after extrusion and provides a fast stress healing property. For the developed system, the unjammed microgels recovered almost immediately after removing the shear and switched to the original viscoelastic state from an as-prepared fluid in a short time (5 s, Fig. 2-c). For G-gel $_{I}$, the modulus exhibited a decreasing trend from cycle 1 to cycle 4 with a

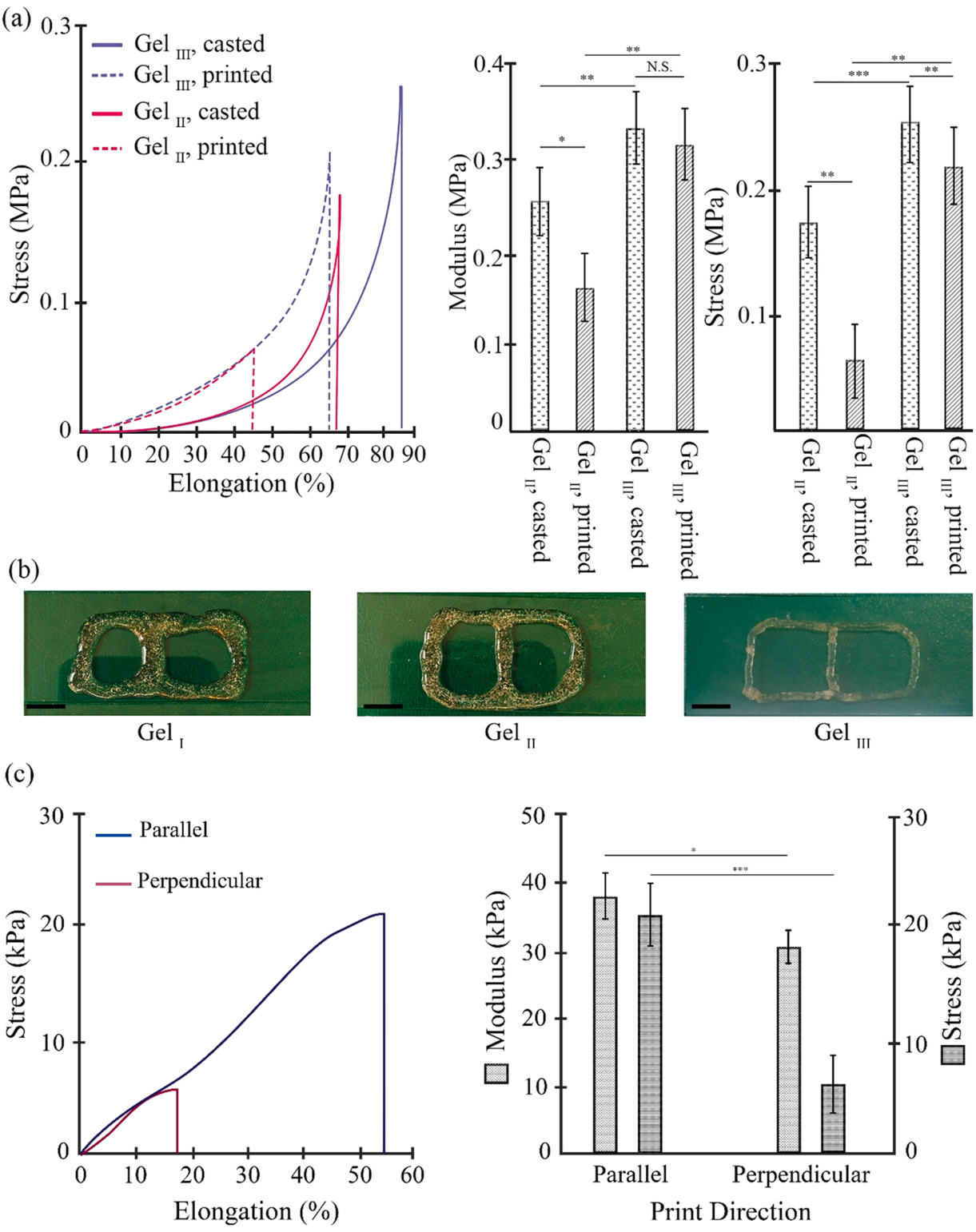

Fig. 4. (a) Representative Stress-Elongation curves for the casted and printed samples in longitudinal and transversal orientations with G-gel $_{II}$ and G-gel $_{III}$. For measurement, the printed cubic samples are punched to a cylindrical shape with the same shape and size as casted samples. (b) Spreading and shape-retaining properties of inks as they reach to a glass substrate. Scale bar is 10 mm. (c) The effect of printing direction on tensile properties of G-gel $_{III}$.

significant decrease after cycle 3. However, G-gel $_{II}$ and G-gel $_{III}$ displayed a reproducible and stable characteristic during four stress-relaxation cycles indicating the performance of rupture and reformation of superficial hydrophobic interactions during the process. We concluded that the attraction of particles enhances the fast recoverability of viscoelastic properties. The sliding of particles and reformation of interactions within the structure has provided a dissipating morphology, and consequently a tough and fast recoverable material was obtained.

For pure gelatin hydrogel, it has been accepted that the formed network (helical molecules) liquefies at around 30–35 ℃ and converts to random coils when the temperature exceeds the UCST. To test the effect

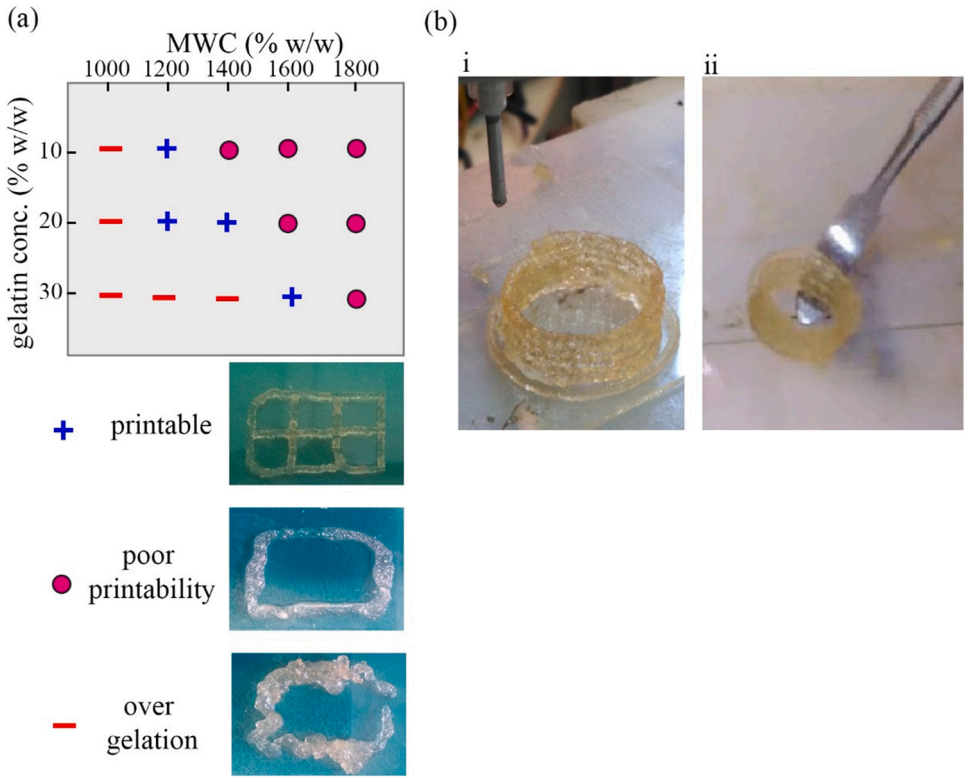

Fig. 5. (a) Printability chart of G-gel $_{III}$ in terms of microgel water content and gelatin fraction. Over gelation or spreading occur if the gelatin is used at higher and lower critical concentration. (b) Designed tubular shape printed by ink G-gel $_{III.}$ (G16 nozzle). The construct is strong due to the attraction among particles and gelation of gelatin, and can be chemically crosslinked when is exposed to the eutectic mixture.

of gelatin network transition as one of the two main components of the prepared ink, a temperature sweep rheometery was performed at 25–55 ℃. It was observed that the storage modulus was still higher than loss modulus, and therefore the filaments could preserve their strength despite the transition of gelatin at 32 ℃ (Movie S-2, supplementary information). Indeed, the attraction of microgels prevents the collapsing of construct and guarantees the stability of the extruded filaments.

Shear-thinning behavior contributes to printability, but may be undesirable for shape fidelity after extrusion. Shear thinning hydrogels may have poor recoverability, so that the ink will spread as it reaches the substrate preventing fast recoverability. Generally, the fidelity of inks can be evaluated by their capability to produce filaments stable against their own weight (Fig. 3-a) [6]. The extruded filaments may creep or collapse by their own weight. To quantify the ability of our ink to self-support under applied stress, a creep test was performed on the G-gel $_{II}$ and G-gel $_{III}$. A constant stress was applied and the strain was continuously recorded over time. The microgels with different length of hydrophobic PGMA segments underwent different rates of strain evolution, as shown in Fig. 3-b. G-gel $_{III}$ exhibited 0.21% deformation in about 60 s, while G-gel $_{II}$ underwent 0.62% deformation at the same time. Indeed, G-gel $_{III}$ has shown better self-supporting property and resistance against the constant stress. This indicates clearly the viscoelastic character of the samples, i.e. the elasticity increases with increasing in length of hydrophobic segment. Movies S-3 to S-5 (Supplementary Information) present the self-supporting and fast recovery nature of these gels, which are critical parameter for the shape fidelity of printed constructs. After minutes, the strain evolution began a decreasing trend when the gelation of gelatin molecules was commenced (Fig. 3-b). This phenomenon was also apparent in strain variation of single filament after few minutes, as shown in Fig. 3-c. It should be added that water evaporation had also additional impact on shape changes of a single filament, otherwise the shown changes in Fig. 3-c was in contrast with shape fidelity.

Another challenge related to shape fidelity, especially if the construct is composed of more than a few layers, is the weakness of the structure to withstand multiple layers on top of each other and sustain the formation of a bulk volumetric construct. This is because of the intrinsic layer-by-layer fabrication process, such that the weak bond strength between the printed layers results in delamination and poor mechanical properties. Depending on the gelation mechanism, interfaces may form between layers located on top and adjacent of the previously deposited line instead of homogeneous coalescence, leading to the formation of an anisotropic morphology [49]. These interfaces result in structural defects and pulling the layers apart when the 3D printed construct is under loading of the upper layers. The methodology proposed in this study follows a process through which the newly depositing layer adheres to the adjacent lines with insignificant interface formation. To test whether hydrophobic segments of the previously deposited layer are able to associate with adjacent segments, the stiffness of the casted and the printed cylindrical specimens were measured using compression testing. The compression strength of the printed samples was determined as 0.06 and 0.21 MPa for G-gel $_{II}$ and G-gel $_{III}$, respectively, lower than that of corresponding casted samples (0.17 and 0.26 MPa for G-gel $_{II}$ and G-gel $_{III}$, respectively) (Fig. 4-a). For G-gel $_{III}$, the obtained compression stress-strain curves showed more similar mechanical properties, with stress and modulus difference for casted and printed G-gel $_{III}$ samples lower than those of G-gel $_{II}$, indicating better coalescence of the adjacent lines and better adhesion than G-gel $_{III}$ printed layers. In brief, although the mechanical properties of printed samples were weaker compared to the corresponding casted (bulk) counterparts, the modulus and strength of printed G-gel $_{III}$ were closer to casted samples. Moreover, when the ink reached the substrate, spreading was affected by both the interfacial tension between ink material and the substrate, as well as the tension within the material. The images in Fig. 4-b show the behavior of G-gel $_{I,}$ $_{II,}$ $_{III}$ as they get in contact with the substrate. Among three applied microgels, the biomaterial ink based on M-gel $_{III}$ exhibited good

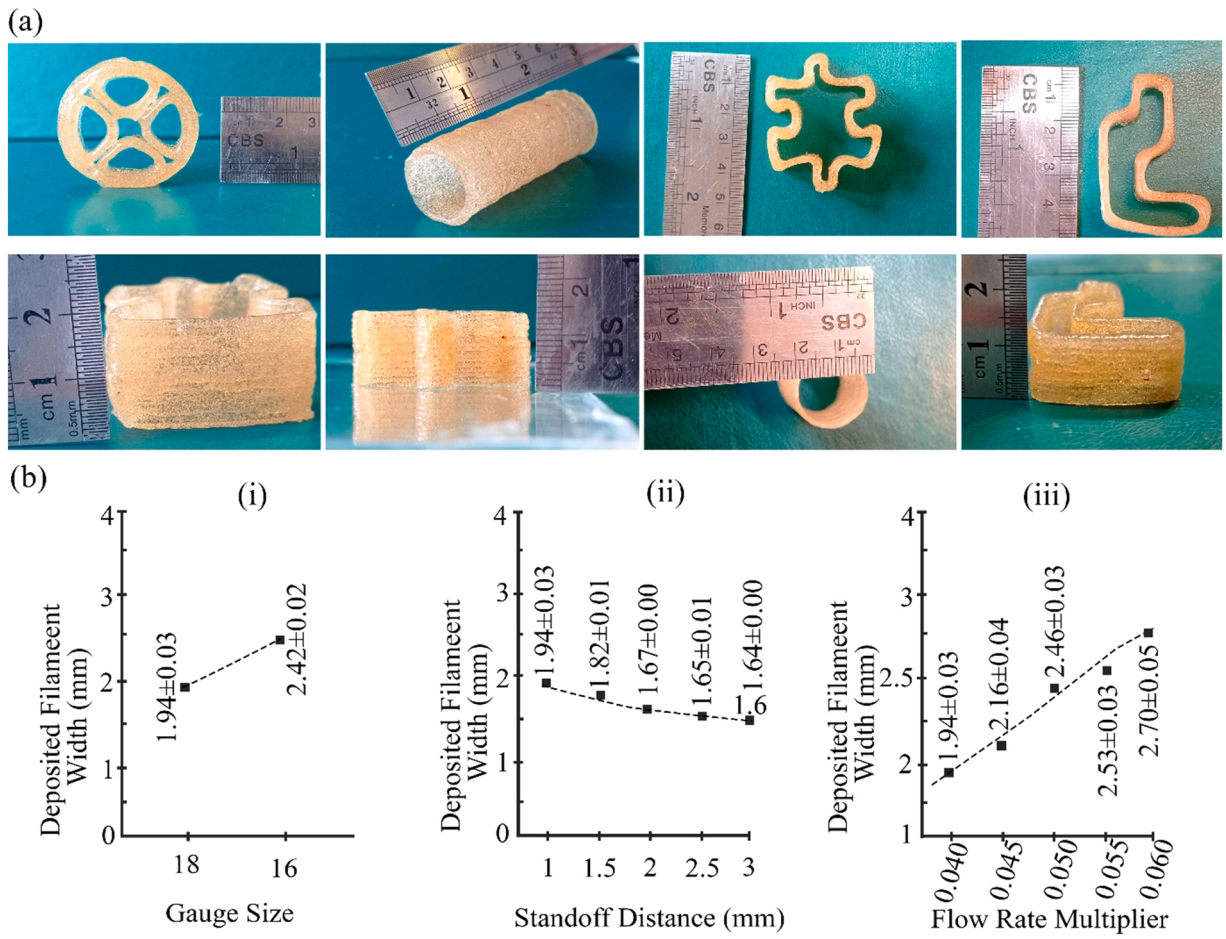

Fig. 6. (a) Photograph of printed jammed microgels extruded from a 18 G nozzle and a travel speed of 2 mm/s. The constructs composed of large number of layer (57 layer in the case of a cylinder for instance) display mechanical integrity after deposition of nearly 12 mL of ink. (b) The influence of processing conditions including (i) different size needles (flow rat multiplier: 0.04 and strand distance: 1 mm), (ii) strand distance (nozzle type: 18 G and flow rate multiplier: 0.04) and (iii) extrusion rates (nozzle type: 18 G and strand distance: 1 mm) on the cross-sectional diameters of deposited filaments on glass.

shape-retaining properties when printed on a glass platform, indicating the presence of sufficient inter-particle attractions. Mechanical properties of the G-gel $_{III}$ were investigated after depositing of filaments in two perpendicular and parallel directions relative to the applied tensile stress. Tensile strength of the sample oriented vertically (6.50 ± 2.50 kPa) was lower compared to the structure in which the orientation was parallel to the stress (20.63 ± 3.06 kPa), which is consistent with mechanical properties of gelatin-based hydrogels [15]. This indicates that although G-gel $_{III}$ possesses required adhesion between the particles, this amount of adhesion is not as strong as covalent interactions, but is enough to keep the as-etruded particles on the previous layers.

Microgel water content (MWC) is a critical parameter for the possibility of formation of hydrophobic interactions [28]. To achieve a strong and self-supporting 3D printed construct, water content and gelatin concentration must be optimized depending on MWC. G-gel $_{III}$ was selected for this investigation and it was found that the concentration of gelatin could be reduced to 10% w/w by decreasing MWC to 1200% (Fig. 5-a). Particularly, when MWC reached 1800% w/w, the ink exhibited a liquid state whereas the other inks with MWC= 1000% w/w were transferred into a gel state before extrusion. Fig. 5-b-i show a tubular structure manufactured by mixing microgels with MWC= 1400% w/w with 20% w/w of gelatin. The obtained construct was strong, could be removed from the surface and handled without any additional crosslinking step (Fig. 5-bii).

To explore the performance of the developed ink for printing applications, the resulted ink containing microgels and pure gelatin was extruded through a G18 nozzle to fabricate structures composed of numerous layers of filaments and several complexities, such as sharp corners and curves (Fig. 6-a). Due to desired strength and shape retaining properties of the ink, the extruded material could adhere to previously deposited layers with retaining the feature sharpness in the corners. No support material or post-crosslinking were required to apply and keep the construct strength against bending, or collapsing after extrusion, resulting in structural fidelity after deposition of a large number of layers. 3D printed hydrogels with large aspect ratio are usually collapsed if they are not crosslinked efficiently by UV-illumination or other methods, but jammed microgels could remain stable after being printed into at least 57-layer cylinders with the height of 54 mm. However, it should be stated that narrower nozzles could not be used for this range of microgel size. For specific applications, using microgels with smaller size would be applicable to increase the resolution of the printed constructs.

The influence of printing parameters, including needle sizes, extrusion rates, and strand distance were investigated on the diameters of extruded filaments. G18 and G16 nozzles were applied to investigate the effect of the size of nozzle on filament diameter. The diameters of the extruded filaments were increased from 1.94 ± 0.03 mm to 2.42 ± 0.02 mm when the G18 and G16 nozzles were applied, respectively.

To explore the effect of strand distance, the distance of tip to glass substrate was adjusted between 1 and 3 mm and filament extruded through a G18 nozzle. It was observed that the filament diameter decreased from 1.9 mm to 1.6 mm when the distance between the

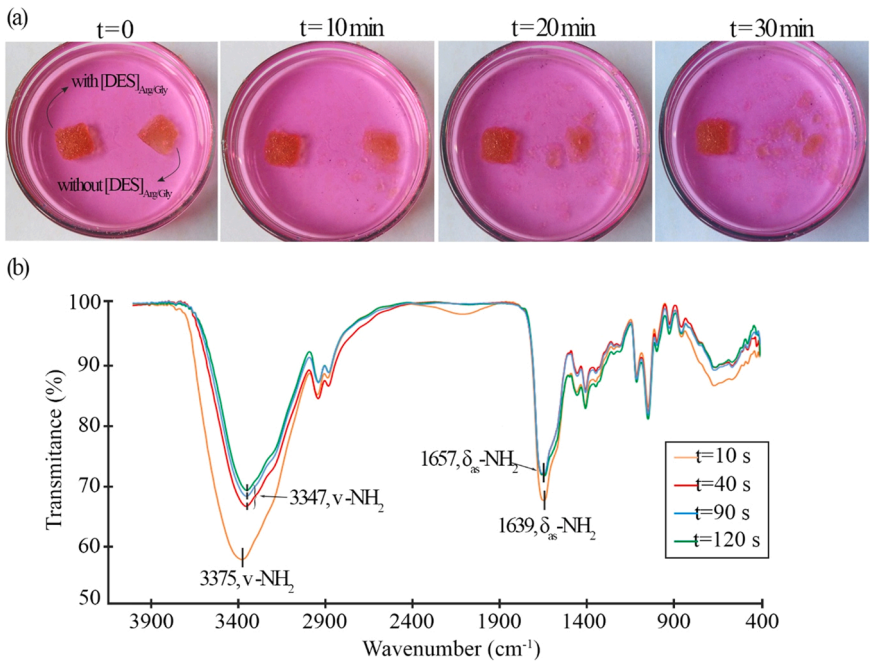

Fig. 7. (a) Effect of chemical crosslinking on the stability of the printed construct at 37 °C. Crosslinking is performed by applying $[DES]_{Arg/Gly}$ on the sample with dimensions of 10 × 10 × 4 mm. (b) The kinetic of crosslinking reaction is investigated by in-situ FT-IR spectroscopy. This reaction involves ring opening of M-gel $_{III}$ epoxy groups by amine groups, which occurs at ambient condition in the presence of $[DES]_{Arg/Gly}$.

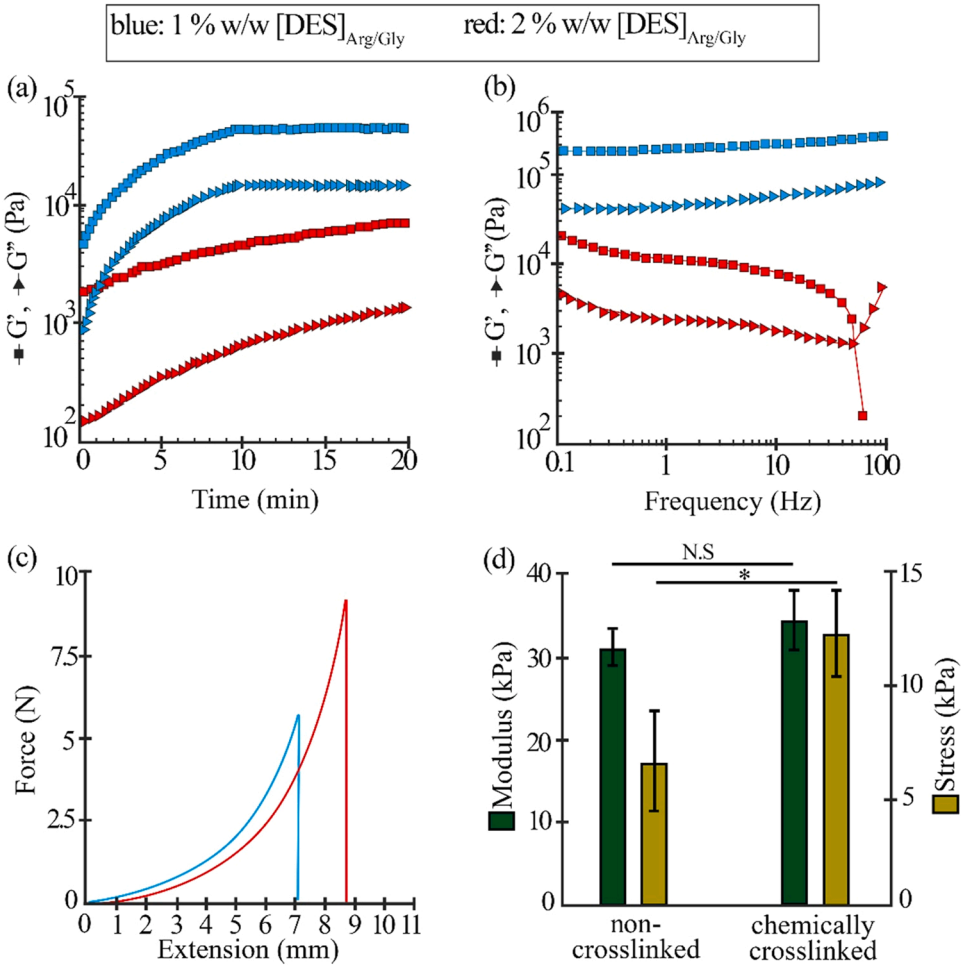

Fig. 8. The role of $[DES]_{Arg/Gly}$ loading concentration on the crosslinking reaction progress and the mechanical properties of the crosslinked specimens. (a) The rate of G' evolution for the mixture of G-gel $_{III}$ and $[DES]_{Arg/Gly}$ indicates the importance of $[DES]_{Arg/Gly}$ concentration on the crosslinking progress. (b) Oscillatory frequency sweep performed on the 3D printed cubic samples crosslinked by applying different volume of $[DES]_{Arg/Gly}$ aqueous solution. (c) Result of compression test performed on cylindrical crosslinked samples prepared by different volume of pure $[DES]_{Arg/Gly}$. (d) Tensile properties of crosslinked and non-crosslinked Gel $_{III}$ printed in perpendicular direction with respect to tensile stress. 1% w/w $[DES]_{Arg/Gly}$ was applied on the printed sample.

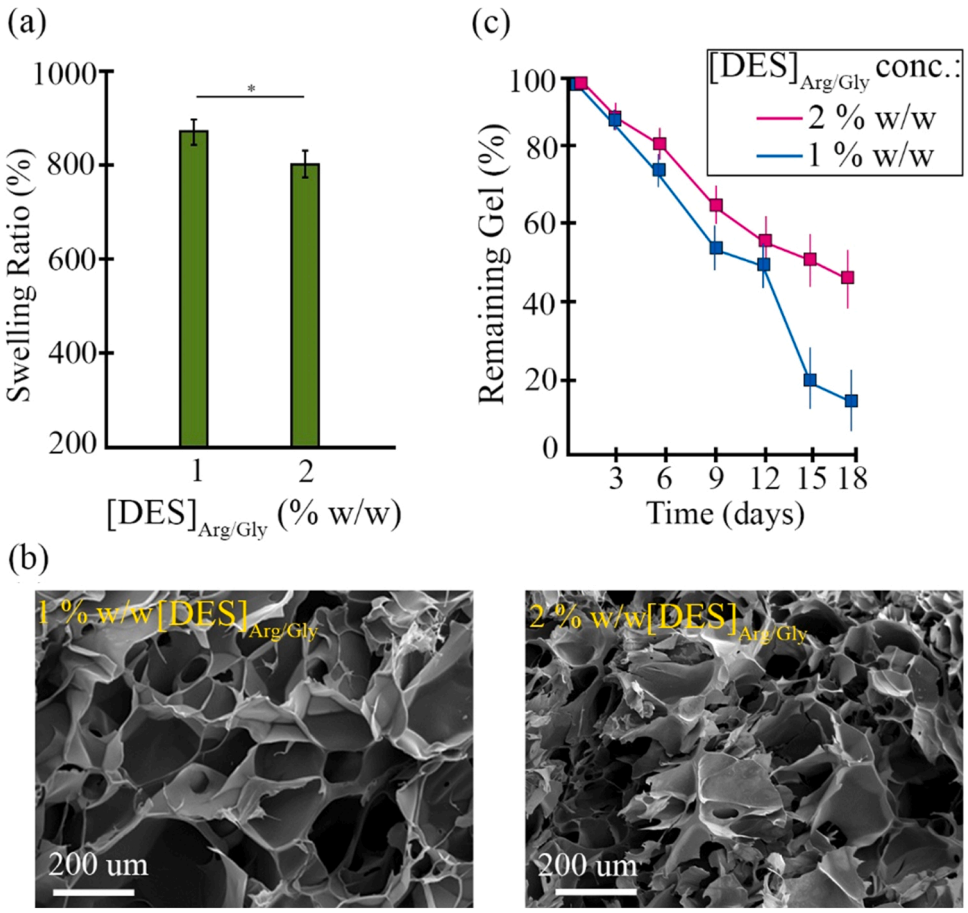

Fig. 9. $[DES]_{Arg/Gly}$ concentration influences (a) hydrogel swelling ratio, (b) morphology and (c) biodegradability of the chemically crosslinked 3D printed objects. The swelling ratio and degradability rate were measured for the samples with dimensions 10 × 10 × 4 mm, crosslinked by applying $[DES]_{Arg/Gly}$ solution on the samples.

needle and printing bed increased to 2 mm. Afterwards, the filament diameter remained constant when the distance increased to 2.5 mm and 3 mm. Based on the observation, it can be concluded that a 2 mm distance is enough for the microgels to aggregate and create the possible narrowest diameter (Fig. 6-b-ii).

The flow rate of the extrusion is also a critical feature on the size of extruded filaments, since higher extrusion rates limit the required time for the ink components to interact. The results regarding the optimization of the flow rate exhibited that a flow rate multiplier of 0.04 led into narrower filaments, and the diameter was increased with the increase of flow rate multiplier (Fig. 6-b-iii).

3.2. Synthesis of $[DES]_{Arg/Gly}$ for chemical crosslinking

$[DES]_{Arg/Gly}$ was obtained by interaction of Arg with –OH groups of glycerol under atmospheric pressure conditions, 120 ℃ for 25 min, which resulted in a brown viscous liquid. Fig. S1 shows the structure and synthesis path of $[DES]_{Arg/Gly}$ formation. From the point of view of hydrogen bond formation, glycerol carries three close –OH groups through which the intermolecular ionic interactions within the arginine can be easily interrupted. The raw materials were mixed at different molar ratios and their physical properties were assessed to obtain the eutectic point. Using Arg:Gly at 1:0.5 molar ratio, even at longer reaction times, a dark pasty-like solid was obtained and discarded from subsequent evaluation. The other mixtures provided a room temperature stable liquid and were assessed by density and viscosity measurements to confirm the eutectic point. The lowest density and viscosity were 1.33 g/cm^3 and 1200 cP, respectively in 1:2 molar ratio, as shown in Fig. S2-a. These data suggest the formation of a 1:2 complex between parts of amino acid molecules and –OH groups of Gly molecules (Fig. S1), which is a common behavior in the formation of eutectic mixtures [29,32]. It should be noted that the viscosity value keeps a decreasing trend up to 1:4 molar ratios, which is due to the dissolution of eutectic mixture in excess glycerol.

A 1:2 molar ratio was selected as the eutectic mixture and FT-IR and ^{1}H NMR spectroscopies were used to characterize the interaction between DES components and the appearance of new interactions. For Gly, the –O-H stretching characteristic peak appeared at 3367 cm^{-1}, which shifted to 3355 cm^{-1} in the formed DES, indicating the formation of hydrogen bonds between the components (Fig. S2-b). The vibration for –N-H at 1678 cm^{-1} in the Arg showed a red shift to 1671 cm^{-1} in the $[DES]_{Arg/Gly}$. These results confirmed the formation of intermolecular interactions between Arg and Gly, which was necessary for the formation of the eutectic mixture.

^{1}H NMR was used to follow the changes in interactions during eutectic formation. $[DES]_{Arg/Gly}$ was diluted in D_2O and the obtained spectrum was compared with the primary mixture (a mixture of 1:2 ratio of feed components without eutectic formation) with the same molar ratio and concentration. The integral of the appeared signals in the $[DES]_{Arg/Gly}$ was almost the same with the primary mixture and was equal to the utilized 1:2 molar ratio. It could be deduced that a complex eutectic structure was formed by intermolecular physical interactions without degradation of feed components or formation of possible ester groups.

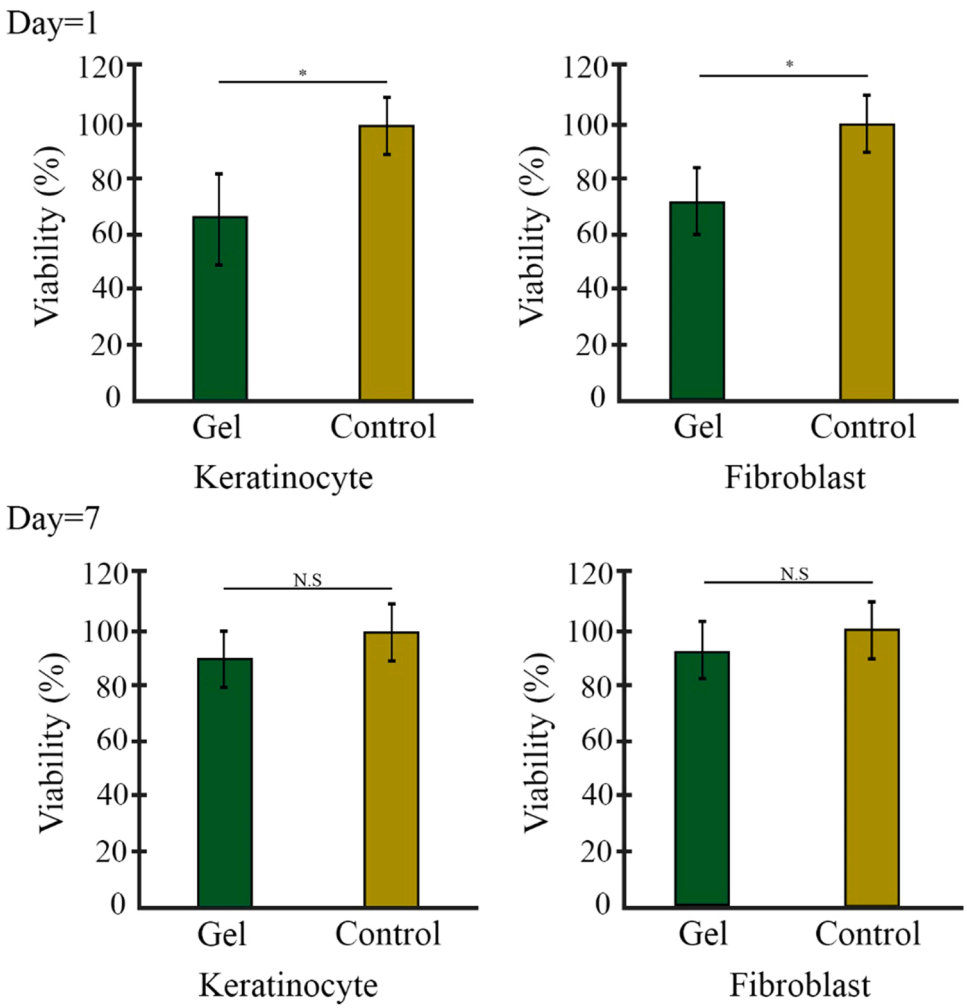

Fig. 10. The relative viability of Fibroblast and Keratinocyte cells compared to the control assessed by the direct contact of cells within the network by MTT assay after 1 and 7 days (n = 3).

3.3. *Catalytic efficiency of [DES]$_{Arg/Gly}$ to trigger chemical crosslinking*

To assess the importance of chemical crosslinking as well as catalytic efficiency of [DES]$_{Arg/Gly}$ to trigger chemical crosslinking, two pieces of 3D printed cubic G-gel $_{III}$ samples were immersed in culture medium, in which one piece has been previously crosslinked by applying [DES]$_{Arg/Gly}$ over the construct. The chemically crosslinked construct retained its shape and integrity even if the temperature increased up to 45 ℃, but the specimen formed with only physical interactions fragmented within 30 min at the same condition, as shown in Fig. 7-a. This confirmed the formation of chemical crosslinks in the presence of [DES]$_{Arg/Gly}$, and also demonstrated that the chemical junctions prevented dissolving of the construct and enhanced shape stability.

In-situ FT-IR spectroscopy and time-sweep rheometery were used to investigate the kinetic of crosslinking reaction in the presence of [DES]$_{Arg/Gly}$. To observe the variation of characteristic peaks during crosslinking, a thin layer of ink material was placed on a KBr disc and the first scan was immediately performed after [DES]$_{Arg/Gly}$ was added. The subsequent scans were performed at different times as shown in Fig. 7-b (10 s is the time needed to run the device). A remarkable difference was observed for the intensity of –NH_2 stretching peaks around 3375 cm^{-1}. This significant decrease was due to the consumption of gelatin amine groups by the reaction with the microgel epoxy groups. Moreover, comparing the second scan (40 s) with the first (10 s) and third (90 s) scans, indicated that the majority of crosslinking reaction was performed within 30–40 s after [DES]$_{Arg/Gly}$ was applied. It was deduced that the degree of reaction reaches to maximum accessible level after 90 s, since no specific changes were observed afterwards. Currently, the reaction of amine with epoxy groups has not been reported at ambient conditions with such a fast rate. The obtained results indicate that the developed [DES]$_{Arg/Gly}$ can be considered as an efficient catalyst to trigger the reaction of –NH_2 nucleophile group with epoxide ring, the reaction desired for chemical crosslinking of microgels.

To get deeper insight into the role of [DES]$_{Arg/Gly}$ on the rate of crosslinking reaction, [DES]$_{Arg/Gly}$ aqueous solution (50/50 v/v) was used at two typical concentrations (1% and 2% w/w with respect to ink) and time sweep rheometery was run to follow the evolution of the viscoelastic parameters. As depicted in Fig. 8-a, G' and G" were measured for 20 min at 25 °C. Under these conditions, both systems showed an increase in G' value as the reaction progressed, indicating that the crosslinking occurred. For the sample with 1% w/w [DES]$_{Arg/Gly}$, the slope of the graph exhibited a significant sharpness in the initial reaction times (∼ min), decreasing thereafter over time. This suggests that the rate of the crosslinking reaction is much higher than that of the sample with doubled [DES]$_{Arg/Gly}$ concentration, which displayed a uniform trend in the first 20 min time period. After 20 min of reaction, the sample with 1% w/w [DES]$_{Arg/Gly}$ reached a storage modulus of 60 kPa, while the latter reached a storage modulus of 5 kPa. Fig. 8-b presents the plot of G′ versus the oscillatory frequency and the obtained data revealed a significant difference between these two samples. With 1% w/w [DES]$_{Arg/Gly}$, the storage modulus exhibited a plateau in the 0.1–100 Hz, which was indicative of a stable cross-linked network [50].

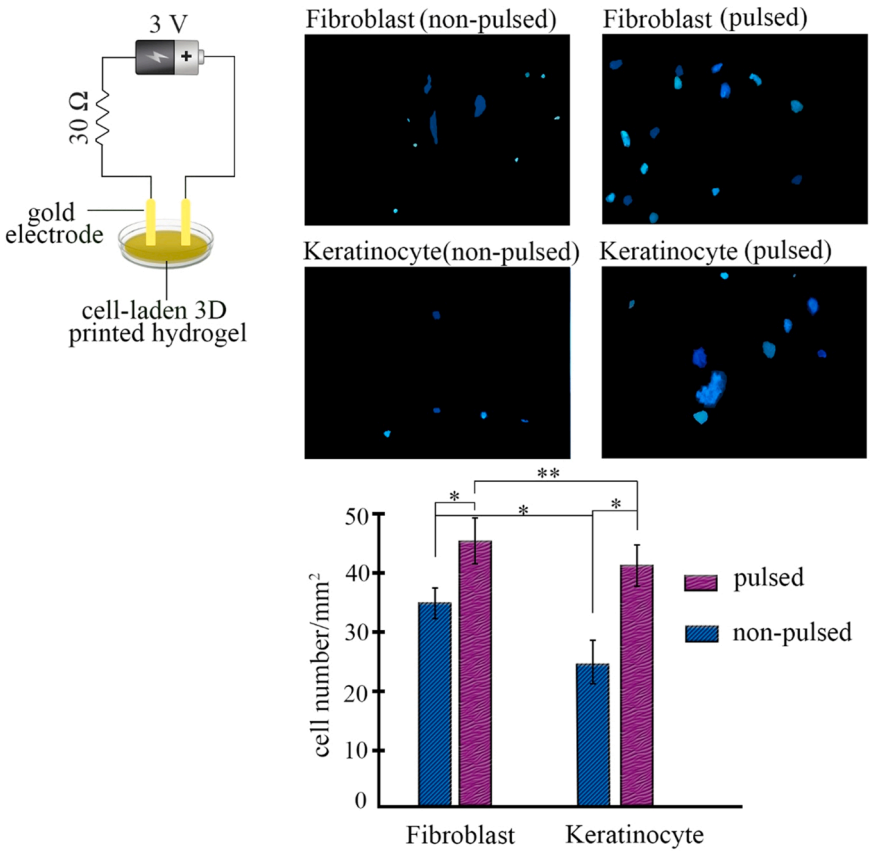

Fig. 11. The images of DAPI staining of Fibroblast and Keratinocyte cells with and without ES (10 min/day) after 7 days (n = 3).

This frequency-independent feature also indicated a solid-like behavior in the cured systems. Although both samples had elasticity dominated properties up to higher frequencies, the sample with 2% w/w $[DES]_{Arg/Gly}$ showed a decreasing trend when the frequency increased. These results were in contrast with our expectation, since the higher loading of catalyst was expected to result in a higher degree of crosslinking and subsequent higher strength. It was believed that the water molecules in $[DES]_{Arg/Gly}$ solution interrupted the attraction of microgels and weakened the formed network. To test our hypothesis, we prepared bulk samples by mixing pure $[DES]_{Arg/Gly}$ (with the same equivalents) with ink material instead of using $[DES]_{Arg/Gly}$ aqueous solution, and did compression test (Fig. 8-c). A higher loading of $[DES]_{Arg/Gly}$ resulted in a higher strength (9.1 N) and toughness than the latter, whose strength was only 5.6 N. These superior mechanical properties were likely related to a higher degree of crosslinking offered by the catalytic efficiency of pure $[DES]_{Arg/Gly}$ and proved our hypotheses that water molecules affected the mechanical properties. The tensile properties of chemically crosslinked structures were compared with those before applying $[DES]_{Arg/Gly}$. It was observed that the tensile strength of samples increased from 6.50 ± 2.50 kPa to 10.25 ± 3.85 kPa (Fig. 8-d).

In addition to the crosslinking rate, the physiochemical properties and microstructure of the final hydrogels are critical parameters, which are affected by $[DES]_{Arg/Gly}$ concentration since crosslinking density depends on the number of formed covalent bonds. Different swelling behavior, morphology and degradability rate were observed depending on $[DES]_{Arg/Gly}$ concentration (Fig. 9). The maximum amount of water uptake was measured as 886% and 794% for the networks crosslinked with 1% and 2% w/w $[DES]_{Arg/Gly}$, respectively. SEM images confirmed the effect of $[DES]_{Arg/Gly}$ loading concentration on the microstructure of the network (Fig. 9-b). A relatively denser morphology was found for the samples obtained by 2% w/w $[DES]_{Arg/Gly}$. Indeed, the swelling ratio was affected by porosity, and the porosity was dependent on $[DES]_{Arg/Gly}$ concentration. Moreover, the degradation rate is also important for tissue engineering scaffolds, which depends on the degree of crosslinking. Degradation results of the hydrogels indicated a faster degradation rate for the samples with lower crosslinking density (Fig. 9-c). Indeed, the degradation rate of the 3D printed objects could be adjusted by the amount of $[DES]_{Arg/Gly}$ applied. According to these findings, the performance of $[DES]_{Arg/Gly}$ was affected by the applied concentration and crosslinking conditions such as using pure $[DES]_{Arg/Gly}$ or its aqueous solution. In this work, the applied concentrations of $[DES]_{Arg/Gly}$ solution were only for evaluating and demonstrating the efficiency, performance and effect of $[DES]_{Arg/Gly}$ on the properties of 3D printed construct. Therefore, it is suggested that for 3D printing of objects with different dimensions and geometries, $[DES]_{Arg/Gly}$ application must be considered and optimized accordingly to obtain practical additive manufactured structures.

3.4. *Viability and in vitro cellular stimulation*

Conductive biomaterials are considered as attractive materials, have gained increasing interest since they provide a cell-effective environment, and can mimic the natural electrical and biological characteristics of the tissues [51,52]. Many relevant studies have designed conductive platforms that are useful to promote the formation of functional tissues. As the cell signaling pathways can be regulated via biological electrical signals, myotube formation and cell proliferation are affected in the presence of electrical stimulation (ES) [53,54]. *In vitro* investigations have proved that ES can enhance migration and proliferation of cells and secretion of more extracellular matrix for tissue regeneration [55]. Although DESs were initially introduced as high-potential candidates in the preparation of innovative materials, their use in the preparation of ionic soft materials can be considered as a new research topic. It was

believed the incorporation of $[DES]_{Arg/Gly}$ could provide a conductive platform, and subsequently stimulate the cells if electrical pulses were applied. To evaluate this, the viability of fibroblasts and keratinocytes was first examined. As shown in Fig. 10, cell viability decreased after 1 day of mixing the ink precursor with both cells. This might be attributed to different reasons, such as cell death during extrusion through nozzle and higher polarity of the eutectic mixture; however, direct contact between cells and hydrogels after 7 days did not significantly alter cellular activity. We conducted a further *in vitro* assay to electrically stimulate fibroblasts and keratinocytes proliferation (Fig. 11). The electrodes were in direct contact with the culture medium during ES application and were removed after application. An accelerated proliferation of fibroblasts and keratinocytes was observed after the application of ES for 7 days, for 10 min/day. DAPI staining confirmed that ES could significantly increase cell proliferation in the stimulated group compared to the non-stimulated condition. Cell counting showed that the proliferation rate of keratinocytes was higher than fibroblasts at the same time and stimulation conditions. It could be concluded that the presence of $[DES]_{Arg/Gly}$ and application of electrical pulses enhance cell proliferation indicating the important role of hydrogel conductivity to stimulate cells. These results confirm previous reports indicating that the cellular metabolic activity of fibroblasts is enhanced by ES application [55,56].

4. Conclusion

The concept of using the jammed state of decorated microgels is introduced, which results in a self-supporting structure and improves shape fidelity of 3D printed structures. This is associated to a continuous and steady flow of the jammed microgels, and a rapid recovery/setting. 3D printed constructs are initially composed of physical crosslinking, which are formed immediately after the extruding process, followed by a chemical crosslinking. The presence of hydrophobic segments over the microgels enhances the attraction of particles, and consequently the rheological properties and printability of the prepared ink are affected. For chemical crosslinking, a new approach is provided by applying $[DES]_{Arg/Gly}$ to trigger fast covalent network formation. Importantly, the applied eutectic mixture provides control and versatility on crosslinking kinetic, mechanical and physiochemical properties, and microstructure of network depending on $[DES]_{Arg/Gly}$ concentration. With this flexibility, it is possible to control the properties of 3D printed constructs. Finally, the presence of $[DES]_{Arg/Gly}$ opens up new possibilities to design conductive soft materials, which are promising method to fabricate the materials with various functionalities.

Supporting Information

Supporting Information is available from the Elsevier Online Library or from the author.

CRediT authorship contribution statement

Moroni Lorenzo: Writing – review & editing, Validation, Supervision. **Ghodsi Saman:** Methodology, Investigation. **Rafiemanzelat Fatemeh:** Writing – review & editing, Validation, Supervision, Software, Resources, Project administration, Funding acquisition, Data curation, Conceptualization. **Sheikhi Mehdi:** Writing – original draft, Visualization, Software, Methodology, Investigation, Formal analysis, Data curation, Conceptualization. **Setayeshmehr Mohsen:** Writing – review & editing, Validation.

Declaration of Competing Interest

The authors declare that they have no known competing financial interests or personal relationships that could have appeared to influence the work reported in this paper.

Data availability

Data will be made available on request.

Acknowledgments

Appreciation is extended to the Office of Vice Chancellor for Research and Technology of University of Isfahan, Iran; and Iran National Science Foundation, Iran for financial supporting of this work (No. 99026593). We also extend our thanks to Dr. Ahmad-Reza Askari for his constructive advices in statistical analysis. Technical support of Miss. Firoozeh Kavosh Tehrani is also acknowledged.

Appendix A. Supporting information

Supplementary data associated with this article can be found in the online version at doi:10.1016/j.addma.2022.102997.

References

[1] C. Mota, S. Camarero-Espinosa, M.B. Baker, P. Wieringa, L. Moroni, Bioprinting: from tissue and organ development to in vitro models, Chem. Rev. 120 (2020) 10547–10607, https://doi.org/10.1021/acs.chemrev.9b00789.
[2] S. Naghieh, D. Chen, Printability–a key issue in extrusion-based bioprinting, J. Pharm. Anal., J. Pharm. Anal. (2021), https://doi.org/10.1016/j.jpha.2021.02.001.
[3] A. Babbar, A. Sharma, R. Kumar, P. Pundir, V. Dhiman, Functionalized biomaterials for 3D printing: An overview of the literature, Addit. Manuf. Func. Nanomater (2021) 87–107, https://doi.org/10.1016/B978-0-12-823152-4.00005-3.
[4] T. Li, J. Chang, Y. Zhu, C. Wu, 3D printing of bioinspired biomaterials for tissue regeneration, Adv. Healthc. Mater. 9 (2020), 2000208, https://doi.org/10.1002/adhm.202000208.
[5] U. Jammalamadaka, K. Tappa, Recent advances in biomaterials for 3D printing and tissue engineering, J. Funct. Biomater. 9 (2018) 22, https://doi.org/10.3390/jfb9010022.
[6] A. Schwab, R. Levato, M. D'Este, S. Piluso, D. Eglin, J. Malda, Printability and shape fidelity of bioinks in 3D bioprinting, Chem. Rev. 120 (2020) 11028–11055, https://doi.org/10.1021/acs.chemrev.0c00084.
[7] M. Setayeshmehr, S. Hafeez, C. van Blitterswijk, L. Moroni, C. Mota, M.B. Baker, Bioprinting via a dual-gel bioink based on poly vinyl alcohol and solubilized extracellular matrix towards cartilage engineering, Int. J. Mol. Sci. 22 (2021) 3901, https://doi.org/10.3390/ijms22083901.
[8] D. Nahm, F. Weigl, N. Schaefer, A. Sancho, A. Frank, J. Groll, R. Luxenhofer, A versatile biomaterial ink platform for the melt electrowriting of chemically-crosslinked hydrogels, Mater. Horiz. 7 (2020) 928–933, https://doi.org/10.1039/C9MH01654F.
[9] J.H. Galarraga, M.Y. Kwon, J.A. Burdick, 3D bioprinting via an in situ crosslinking technique towards engineering cartilage tissue, Sci. Rep. 9 (2019) 1–12, https://doi.org/s41598-019-56117-3.
[10] L. Hahn, M. Beudert, M. Gutmann, L. Keßler, P. Stahlhut, L. Fischer, R. Luxenhofer, From thermogelling hydrogels toward functional bioinks: controlled modification and cytocompatible crosslinking, Macromol. Biosci. (2021), 2100122, https://doi.org/10.1002/mabi.202100122.
[11] N. Paxton, W. Smolan, T. Böck, F. Melchels, J. Groll, T. Jungst, Proposal to assess printability of bioinks for extrusion-based bioprinting and evaluation of rheological properties governing bioprintability, Biofabrication 9 (2017), 044107, https://doi.org/10.1088/1758-5090/aa8dd8.
[12] D.C. Corbett, E. Olszewski, K. Stevens, A FRESH take on resolution in 3D bioprinting, Trends Biochem. Sci. 37 (2019) 1153–1155, https://doi.org/10.1016/j.tibtech.2019.09.003.
[13] F. Kreimendahl, C. Kniebs, A.M. Tavares Sobreiro, T. Schmitz-Rode, S. Jockenhoevel, A.L. Thiebes, FRESH bioprinting technology for tissue engineering–the influence of printing process and bioink composition on cell behavior and vascularization, J. Appl. Biomater. Funct. Mater. 19 (2021), https://doi.org/10.1177/22808000211028808.
[14] C.B. Highley, K.H. Song, A.C. Daly, J.A. Burdick, Jammed microgel inks for 3D printing applications, Adv. Sci. 6 (2019), 1801076, https://doi.org/10.1002/advs.201801076.
[15] K. Song, A.M. Compaan, W. Chai, Y. Huang, Injectable gelatin microgel-based composite ink for 3D bioprinting in air, ACS Appl. Mater. Interfaces 12 (2020) 22453–22466, https://doi.org/10.1021/acsami.0c01497.
[16] T. Bhattacharjee, T.E. Angelini, 3D T cell motility in jammed microgels, J. Phys. D. J. Phys. D. Appl. Phys. 52 (2018), 024006, https://doi.org/10.1088/1361-6463/aae813.
[17] L. Riley, L. Schirmer, T. Segura, Granular hydrogels: emergent properties of jammed hydrogel microparticles and their applications in tissue repair and regeneration, Curr. Opin. Biotech. 60 (2019) 1–8, https://doi.org/10.1016/j.copbio.2018.11.001.

[18] A. GhavamiNejad, N. Ashammakhi, X.Y. Wu, A. Khademhosseini, Crosslinking strategies for 3D bioprinting of polymeric hydrogels, Small 16 (2020), 2002931, https://doi.org/10.1002/smll.202002931.
[19] M. Lee, R. Rizzo, F. Surman, M. Zenobi-Wong, Guiding lights: tissue bioprinting using photoactivated materials, Chem. Rev. 120 (2020) 10950–11027, https://doi.org/10.1021/acs.chemrev.0c00077.
[20] L. Ouyang, C.B. Highley, W. Sun, J.A. Burdick, A generalizable strategy for the 3D bioprinting of hydrogels from nonviscous photo-crosslinkable inks, Adv 29 (2017), 1604983, https://doi.org/10.1002/adma.201604983.
[21] J. Gopinathan, I. Noh, Click chemistry-based injectable hydrogels and bioprinting inks for tissue engineering applications, Tissue Eng. Regen. Med. 15 (2018) 531–546, https://doi.org/10.1007/s13770-018-0152-8.
[22] L. Shi, H. Carstensen, K. Hölzl, M. Lunzer, H. Li, J. Hilborn, D.A. Ossipov, Dynamic coordination chemistry enables free directional printing of biopolymer hydrogel, Chem. Mater. 29 (2017) 5816–5823, https://doi.org/10.1021/acs.chemmater.7b00128.
[23] C. Zhao, Z. Wu, H. Chu, T. Wang, S. Qiu, J. Zhou, Y. Bai, Thiol-rich multifunctional macromolecular crosslinker for gelatin-norbornene-based bioprinting, Biomacromolecules 22 (2021) 2729–2739, https://doi.org/10.1021/acs.biomac.1c00421.
[24] H. Jian, M. Wang, Q. Dong, J. Li, A. Wang, X. Li, S. Bai, Dipeptide self-assembled hydrogels with tunable mechanical properties and degradability for 3D bioprinting, ACS Appl. Mater. Interfaces 11 (2019) 46419–46426, https://doi.org/10.1021/acsami.9b13905.
[25] A.K. Das, P.K. Gavel, Low molecular weight self-assembling peptide-based materials for cell culture, antimicrobial, anti-inflammatory, wound healing, anticancer, drug delivery, bioimaging and 3D bioprinting applications, Soft Matter 16 (2020) 10065–10095, https://doi.org/10.1039/D0SM01136C.
[26] F.L. Morgan, L. Moroni, M.B. Baker, Dynamic bioinks to advance bioprinting, Adv. Healthc. Mater. 9 (2020), 1901798, https://doi.org/10.1002/adhm.201901798.
[27] W. Zou, J. Dong, Y. Luo, Q. Zhao, T. Xie, Dynamic covalent polymer networks: from old chemistry to modern day innovations, Adv 29 (2017), 1606100, https://doi.org/10.1002/adma.201606100.
[28] M. Sheikhi, F. Rafiemanzelat, L. Moroni, M. Setayeshmehr, Ultrahigh-water-content biocompatible gelatin-based hydrogels: Toughened through micro-sized dissipative morphology as an effective strategy, Mater. Sci. Eng., C. 120 (2021), 111750, https://doi.org/10.1016/j.msec.2020.111750.
[29] B.B. Hansen, S. Spittle, B. Chen, D. Poe, Y. Zhang, J.M. Klein, J.R. Sangoro, Deep eutectic solvents: A review of fundamentals and applications, Chem. Rev. 121 (2020) 1232–1285, https://doi.org/10.1021/acs.chemrev.0c00385.
[30] P. Kalhor, K. Ghandi, Deep eutectic solvents for pretreatment, extraction, and catalysis of biomass and food waste, Molecules 24 (2019) 4012, https://doi.org/10.3390/molecules24224012.
[31] Y. Marcus, Applications of deep eutectic solvents. Deep Eutectic Solvents, Springer, 2019.
[32] M. Sheikhi, F. Rafiemanzelat, N. Sadeghpour, M. Shams, A.N. Esfahani, Deep eutectic solvents based on L-arginine and glutamic acid as green catalysts and conductive agents for epoxy resins, J. Mol. Liq. (2021), 117568, https://doi.org/10.1016/j.molliq.2021.117568.
[33] S. Talebian, M. Mehrali, R. Raad, F. Safaei, J. Xi, Z. Liu, J. Foroughi, Electrically conducting hydrogel graphene nanocomposite biofibers for biomedical applications, Front. Chem. 8 (2020) 88, https://doi.org/10.3389/fchem.2020.00088.
[34] S. Yang, L. Jang, S. Kim, J. Yang, K. Yang, S.W. Cho, Polypyrrole/alginate hybrid hydrogels: electrically conductive and soft biomaterials for human mesenchymal stem cell culture and potential neural tissue engineering applications, Macromol. Biosci. 16 (2016) 1653–1661, https://doi.org/10.1002/mabi.201600148.
[35] M. Sasaki, B.C. Karikkineth, K. Nagamine, H. Kaji, K. Torimitsu, M. Nishizawa, Highly conductive stretchable and biocompatible electrode–hydrogel hybrids for advanced tissue engineering, Adv. Healthc. Mater. 3 (2014) 1919–1927, https://doi.org/10.1002/adhm.201400209.
[36] S.R. Shin, B. Aghaei-Ghareh-Bolagh, X. Gao, M. Nikkhah, S.M. Jung, Dolatshahi- A. Pirouz, Layer-by-layer assembly of 3D tissue constructs with functionalized graphene, Adv. Funct. Mater. 24 (2014) 6136–6144, https://doi.org/10.1002/adfm.201401300.
[37] R. Balint Cassidy, S.H. Cartmell, Conductive polymers: Towards a smart biomaterial for tissue engineering, Acta Biomater. 10 (2014) 2341–2353, https://doi.org/10.1016/j.actbio.2014.02.015.
[38] J. Foroughi, G.M. Spinks, G.G. Wallace, Effect of synthesis conditions on the properties of wet spun polypyrrole fibres, Synth. Met. 159 (2009) 1837–1843, https://doi.org/10.1016/j.synthmet.2009.06.006.
[39] S. Ahadian, J. Ramón-Azcón, M. Estili, X. Liang, S. Ostrovidov, H. Shiku, Hybrid hydrogels containing vertically aligned carbon nanotubes with anisotropic electrical conductivity for muscle myofiber fabrication, Sci. Rep. 4 (2014) 4271, https://doi.org/10.1038/srep04271.
[40] H. Zong, B. Wang, G. Li, S. Yan, K. Zhang, Y. Shou, J. Yin, Biodegradable High-Strength Hydrogels with Injectable Performance Based on Poly (l-Glutamic Acid) and Gellan Gum, ACS Biomater. Sci. Eng. 6 (2020) 4702–4713, https://doi.org/10.1021/acsbiomaterials.0c00915.
[41] Y. Wang, T. Zhu, H. Kuang, X. Sun, J. Zhu, Y. Shi, T. Hong, Preparation and evaluation of poly (ester-urethane) urea/gelatin nanofibers based on different crosslinking strategies for potential applications in vascular tissue engineering, RSC Adv. 8 (2018) 35917–35927, https://doi.org/10.1039/C8RA07123C.
[42] H. Wei, M. Lei, P. Zhang, J. Leng, Z. Zheng, Y. Yu, Orthogonal photochemistry-assisted printing of 3D tough and stretchable conductive hydrogels, Nat. Commun. 12 (2021) 1–10, https://doi.org/10.1038/s41467-021-21869-y.
[43] C. Aronsson, M. Jury, S. Naeimipour, F.R. Boroojeni, J. Christoffersson, P. Lifwergren, Aili, Dynamic peptide-folding mediated biofunctionalization and modulation of hydrogels for 4D bioprinting, Biofabrication 12 (2020), 035031, https://doi.org/10.1088/1758-5090/ab9490.
[44] L.L. Wang, C.B. Highley, Y.C. Yeh, J.H. Galarraga, S. Uman, J.A. Burdick, Three-dimensional extrusion bioprinting of single-and double-network hydrogels containing dynamic covalent crosslinks, J. Biomed. Mater. Res. 106 (2018) 865–875, https://doi.org/10.1002/jbm.a.36323.
[45] M. Zhou, B.H. Lee, Y.J. Tan, L.P. Tan, Microbial transglutaminase induced controlled crosslinking of gelatin methacryloyl to tailor rheological properties for 3D printing, Biofabrication 11 (2019), 025011, https://doi.org/10.1088/1758-5090/ab063f.
[46] T.M. Valentin, S.E. Leggett, P.Y. Chen, J.K. Sodhi, L.H. Stephens, H.D. McClintock, I.Y. Wong, Stereolithographic printing of ionically-crosslinked alginate hydrogels for degradable biomaterials and microfluidics, Lab a Chip 17 (2017) 3474–3488, https://doi.org/10.1039/C7LC00694B.
[47] J. Wang, S. Stanic, A.A. Altun, M. Schwentenwein, K. Dietliker, L. Jin, Grützmacher, A highly efficient waterborne photoinitiator for visible-light-induced three-dimensional printing of hydrogels, Chem. Comm. 54 (2018) 920–923, https://doi.org/10.1039/C7CC09313F.
[48] L. Xie, X. Xiong, Q. Chang, X. Chen, C. Wei, X. Li, Z. Cui, Inkjet-Printed High-Efficiency Multilayer QLEDs Based on a Novel Crosslinkable Small-Molecule Hole Transport Material, Small 15 (2019), 1900111, https://doi.org/10.1002/smll.201900111.
[49] K. Christensen, B. Davis, Y. Jin, Y. Huang, Effects of printing-induced interfaces on localized strain within 3D printed hydrogel structures, Mater. Sci. Eng., C. 89 (2018) 65–74, https://doi.org/10.1016/j.msec.2018.03.014.
[50] I. Ali, L.A. Shah, Rheological investigation of the viscoelastic thixotropic behavior of synthesized polyethylene glycol-modified polyacrylamide hydrogels using different accelerators, Polym. Bull. 78 (2021) 1275–1291, https://doi.org/10.1016/j.jiec.2016.12.006.
[51] B. Dhandayuthapani, Y. Yoshida, T. Maekawa, D.S. Kumar, Polymeric scaffolds in tissue engineering application: a review, Int. J. Polym. Sci. (2011) 1–20, https://doi.org/10.1155/2011/290602.
[52] K.S. Straley, C.W.P. Foo, S.C. Heilshorn, Biomaterial design strategies for the treatment of spinal cord injuries, J. Neurotrauma 27 (2010) 1–19, https://doi.org/10.1089/neu.2009.0948.
[53] S. Sirivisoot, B.S. Harrison, Skeletal myotube formation enhanced by electrospun polyurethane carbon nanotube scaffolds, Int. J. Nanomed. 6 (2011) 2483, https://doi.org/10.2147/IJN.S24073.
[54] S.R. Shin, S.M. Jung, M. Zalabany, K. Kim, P. Zorlutuna, S.B. Kim, A. Khademhosseini, Carbon-nanotube-embedded hydrogel sheets for engineering cardiac constructs and bioactuators, ACS Nano 7 (2013) 2369–2380, https://doi.org/10.1021/nn305559j.
[55] Y. Wang, M. Rouabhia, D. Lavertu, Z. Zhang, Pulsed electrical stimulation modulates fibroblasts' behaviour through the Smad signalling pathway, J. Tissue Eng. Regen. Med. 11 (2017) 1110–1121, https://doi.org/10.1002/term.2014.
[56] R. Balint, N.J. Cassidy, S.H. Cartmell, Conductive polymers: Towards a smart biomaterial for tissue engineering, Acta Biomater. 10 (2014) 2341–2353, https://doi.org/10.1016/j.actbio.2014.02.015.